Astrophysics Variable Stars Lab

Chris Newey[1]

[1]*SMU Physics Department*

(Accepted April 10, 2020)

Submitted to Prof. Kehoe Physics 3368

ABSTRACT

This project sets out to explore properties of δ Scuti variable stars as well as learn how to use astronomical observation data to find, classify, and analyze variable stars. I use data from ROTSE-I and statistical analysis in order create light light curves which are then manually classified. During this project I was able to identify 27 intrinsic and extrinsic variable stars and determine physical properties. For the intrinsic variable stars I calculated the distance and compared it to the the distance derived from the parallax given by SIMBAD. Notably, for one δ Scuti I found an estimated distance of 904 parsecs compared to 923 parsecs.

1. INTRODUCTION: UNDERSTANDING DELTA SCUTI AND THE FREQUENCIES OF THEIR PULSATIONS

Using astronomical data from the The Robotic Optical Transient Search Experiment (ROTSE-I) telescope, this project will involve identifying and classifying variable stars. Variable stars have light curves which show a periodic change in the apparent brightness of the star and can be broken down into two basic categories, extrinsic and intrinsic variable stars. In our data, the extrinsic stars

cnewey@smu.edu

are eclipsing binaries which consist of two stars orbiting each other. Intrinsic variable stars in our observations consist of stars whose apparent change in brightness will be due to physical properties of the stars themselves (Neilson et al. 2016). The research portion of this project will focus on intrinsic variable stars known as δ Scuti and their pulsation frequencies. In this paper I will concisely cover the interesting physics of δ Scuti stars and their pulsation frequencies, the theoretical problems in recent literature, and the experimental and observational state of the work.

Lying above the main sequence of the Hertzsprung Russel Diagram, δ Scuti display both radial and non-radial pulsations and can be used as standard candles the measure distances. Physically, δ Scuti stars can be dwarfs and giants with spectral types A0–F5 with periods of .3-.03 days and variations in magnitude of 0.003 to 0.9 in the color index V. These variable stars pulsate in multiple pressure (p), gravity (g), and mixed modes with a majority displaying non-radial pulsations. δ Scuti lie on the extension of the Cepheid instability strip towards low luminosities (Balona et al. 2015). Theses stars are significantly dimmer than other variable stars such as δ Cepheid and RR Lyrae. Having narrowed down the classification of δ Scuti, we are able to know the general features including mass, spectral type, and luminosity.

So, the interesting physics lies in explaining the how and why of the pulsations. First, a distinction needs to be made between radial and non-radial pulsations. Radial pulsations occur when the star keeps its spherical shape while swelling and contracting. A non-radial pulsation is when the surface of the star changes topographically, with some parts moving inward and others moving outward. The underlying physics of these stars is referred to as the Kappa Mechanism and is due to large amount of helium in the atmosphere. The helium is heated as it becomes more ionized, which is more opaque. The dimmest part of the star's cycle involves highly ionized opaque helium in its atmosphere increasing the collisions of photons, making it less likely a photon will escape. The energy from the added collisions involving photons causes the helium to heat up, expand, ionize, become more transparent and therefore allow more photons to escape (Templeton 2010). As the star expands and cools the force of gravity inwards overpowers the radiation pressure outward. The cycle of the pulsation continues in an observable periodic fashion.

Once the light curves are created, the frequency analysis involves computer algorithms which utilize both Fourier and multiple-least-squares algorithms. In order to properly identify the pulsation modes, photometry is used to determine the effective temperature, surface gravity, log(g), and the distance modulus. Then the pulsation constant, Q, which is useful in determining the pulsation modes, is calculated using the formula:

$$log\ Q_i = -6.456 + logP_i + 0.5\ log\ g + 0.1M_{bol} + log\ T_{eff} \tag{1}$$

Now, the pulsation mode identification from photometric data uses the pulsation constant, frequency pattern, comparison with models, and an examination of amplitude ratios and phase differences between measurements at different wavelengths (Breger et al. 1993). This research reveals a several layer approach to observing and accurately determining the pulsation modes in δ Scuti. The current research involves applying numerical analysis to astronomical data and comparing the results to previously determined physics theory in order to accurately determine the pulsation modes.

Balona et al. (2015) discuss using photometric data from Kepler in order to learn more about specific frequencies of δ Scuti. This recent research uses the rotational frequency in order to better predict the pulsation frequency distributions. Studying the theoretical effect of rotation combined with theoretical compositions produced less than desirable results which require better modeling and observation. One interesting result is each star has a unique periodogram. The unque periodogram can be used to identify individual stars despite the fact that similar stars have simlar effective temperatures, luminosities and rotational velocities (Balona et al. 2015). This research shows that studying the frequency distributions of δ Scuti creates a new path the better understand the composition and physics in the stars.

In summary, δ Scuti are intrinsic variable stars which are near the main sequence on the Hertzsprung Russel diagram. The interest in δ Scuti comes from the fact that they have periodic pulsations which allow them to be used as standard candles to measure distances in the galaxy. Within the light curve, δ Scuti have pulsation frequencies which can be derived using theoretical models and numerical analysis. From the determination of the pulsation frequency distribution we are able to observe that

otherwise similar stars have distinguishable differences. The research of δ Scuti and their pulsation frequencies allows for a new approach to understanding stellar structure.

2. DETECTOR/APPARATUS

The data for the lab comes from the ROTSE-I instrument. To start, the telescope uses four Canon 200mm f/1.8 unfiltered lenses, each equipped with a thermoelectrically cooled CCD camera with Thompson TH7899M CCD's. The 14 μm pixels of these CCDs subtend 14.4" at this focal length (Akerlof et al. 1994). This system is housed in an electronics enclosure and attached to a mount which is able to slew and track the night sky.

Enabling complete automatic operation, the system consists of five computers one of which is the master computer which checks the weather before beginning nightly operation, keeps track of time, and determines whether the system is in patrol mode or if there is a trigger to search for Gamma-ray bursts. Before opening up for the night the main computer checks for favorable weather conditions. Capable of observing a large field of view, the ROTSE-I sky patrol data images 160 field centers. After slewing to each location, the telescope captures a pair of 80 second exposures in order reduce bad data due to issues such as cosmic rays and hit pixels. In more detail, two patrol sequences are obtained which cover about 18,000 square degrees of sky and record $\approx 9 \times 10^6$ stars with four images (Collaboration et al. 2000).

Conducting all-sky observations in New Mexico starting in March of 1998, ROTSE-I is designed to observe variable stars and Gamma-ray Bursts. The goal of observing Gamma-ray Bursts results in two observation modes for the telescope. Automatic operation consisted of nightly patrol observations which could be interrupted by triggers which shifted the telescope in order to observe Gamma-ray burst. Even though the observation of Gamma-ray bursts took precedence over patrol operation, the regular mode of observation produced a significant amount of variable star data, which this project will analyze.

3. DATA SAMPLES/DATA REDUCTION

Since the telescope relies on CCD's, a systematic analysis of noise counts per pixel needs the be assessed. During the observation process, the telescope takes 12 dark frames which are averaged to provide the median count and then subtracts this count from the night. Furthermore, the telescope accounts for the median brightness of the 90 fields by taking flats which account for sky noise as well as vignetting. So, while the data from the ROTSE-I telescope still requires further analysis and reduction, the combination of dark and flat counts removed from the raw pixel counts of the CCD's provides a reliable source of data for analysis.

Next, after the telescope produces the data for the night having accounted for the darks and flats the data is further processed by the SExtractor package (Bertin & Arnouts 1996). SExtractor is a widely used and thoroughly tested set of programs used to analyze large sets of astronomical images. The algorithm consists of estimating the sky background, thresholding, deblending, filtering of the detections, photometry, and star/galaxy separation. Finally, SExtractor provides us with accurately separated objects with calculated errors.

The next portion of the data reduction is astrometry, transforming the position of the source on the CCD's into astronomical coordinates. This process is accomplished by using a triangle matching routine and interpolating the data to match stars as accurately as possible in the Tycho star catalog. Again, using the Tycho catalog, the experiment determines an absolute magnitude. First, the ROTSE data undergoes photometric calibration. Since ROTSE-I uses unfiltered CCD's, an empirical transformation:

$$m_{ROTSE} = m_v - \frac{m_b - m_v}{1.875} \tag{2}$$

is used. The color-corrected magnitudes are compared to ROTSE-I instrumental magnitudes to set ROTSE-I zeropoints so that the average Tycho star has $m_{ROTSE} = m_v$ (Collaboration et al. 2000). Now, we have the clean data with calculated errors consisting of separated objects with right ascension and declination as well as relative magnitude and time of observation.

The data samples come from a set of nine ROTSE-I sky patrol fields covering ≈ 2000 square degrees we identify periodic variable stars with mean magnitudes between $m_v = 10.0$ and $m_v = 15.5$. The field of view in New Mexico ranges from 150 at -30° to 1100 at the north celestial pole. As this study

includes substantial regions at both low ($b \approx 10°$) and high ($b = 90°$) galactic latitude (Collaboration et al. 2000). The data comes from one camera source, 1b. The dates for the seven nights of data used in this project are the 9^{th}, 10^{th}, 13^{th}, 14^{th}, 15^{th}, 16^{th}, and 17^{th} of April 2000. The data for the 15^{th} was very inconsistent probably due to cloud coverage and caused several stars to have an added gap in the data.

In conclusion, the ROTSE-I telescope consists of four unfiltered lenses attached to CCD cameras providing an automated all-sky observation. The computers on ROTSE-I automate the tracking as well as determining the dark and flat counts of the CCD's. After the data is produced by the experiment it is then reduced using SExtractor and comparing the data to other well-known observations to determine its position and magnitude. In the end this project shows that ROTSE-I provides quality data for observing variable stars.

4. DATA ANALYSIS AND RESULTS

With the final data from the experiment stored and accessible on servers using IDL we begin a methodical hunt for variable stars. Within the IDL protocol we use the 'find_burst' function to create a large list of possible variable stars which we then sort through by hand. The function 'find_burst' relies on three statistical quantities. The first is delta magnitude, $\Delta m = m_{max} - m_{min}$. The second quantity is the significance of the maximum variation: $\sigma_{max} = \frac{(m_{max} - m_{min})}{\sqrt{\epsilon^2_{\max} + \epsilon^2_{\min}}}$. The third quantity is a minimum χ^2 test to quantize how much a light curve deviates from the mean:

$$\chi^2 = \sum \left[\frac{m_i - m_{avg}}{\sigma_i} \right]^2 \tag{3}$$

The find_burst produces a postscript file with objects plotted with errors, statistical+ systematic (Kehoe et al. 2002). For the project I used $\Delta m = .1$, $\sigma_{max} = 3.0$ and $\min\chi^2 = 2.0$ for all nights except the 15^{th}, the night of poor data, which I used $\Delta m = .1$, $\sigma_{max} = 3.0$ and $\min\chi^2 = 1.0$.

After selecting candidate nightly light curves the light curves, the curves are scanned by hand using the principles of confirmation, consistency, and continuity (Fagg et al. 2009). Confirmation means that one night of observation needs to match up statistically to the next observation so that there a no large gaps in a night of observations. Consistency means that the exposures over the night are

statistically compatible and not jumping around creating a nonphysical curve. Continuity requires that apparent variations follow a trend and are not random. Keeping in mind these requirements, the student hand picks variable stars from the ROTSE-I data for one night. After the variable stars are picked out for the first night, I looked for candidates over multiple nights.

Next, the stars are phased using a cubic spline interpolating polynomial. The cubic spline is used in order to determine the period of a variable star. Given $n+1$ data points, $\{x_0, x_1, \ldots, x_n\}$, a cubic spline interpolating polynomial creates a third order polynomial in each of the intervals. Each spline interpolates the endpoints, x_{i-1} and x_i. In order to create the splines we need to be able to solve for the 4(n-1) coefficients. So, the spline fit is chosen such that each of the polynomials have continuity of the polynomial as well as its first and second derivatives at the inner data points. So, $S(x_i^-) = S(x_i^+)$, $S'(x_i^-) = S'(x_i^+)$, and $S''(x_i^-) = S''(x_i^+)$ for $i = 1, \ldots, n-1$. These equations then yield a matrix that needs to be solved since the coefficients need to be found simultaneously.

In order to determine the period of a variable star from the light curve we use a least squares fit,

$$\frac{\partial G}{\partial c_j} \sum_{i-1}^{N} \omega_i [f(x_i) - y_i]^2 = 0 \tag{4}$$

to find a mapping of $x = \omega t \bmod 1$, where ω is the frequency. Now, the coefficients follow $c_i = c_{i \bmod \mathrm{n}}$. This complicates the matrix that needs to be solved in order to determine the coefficients for a cubic spline polynomial with a calculated period. So, more computation time is needed. The variance for the frequency estimation is:

$$\sigma_\omega^2 = \frac{24}{N} \left(\frac{\sigma}{2\pi T A} \right)^2 \tag{5}$$

(Akerlof et al. 1994). In summary, the data analysis uses visual and statistical analysis to yield an efficient and reliable method of determining variable stars and their periods.

Next, the results are analyzed in order to classify their type and to determine physical properties of the system. The first classification is whether the variability is extrinsic or intrinsic. Intrinsic stars have variability due to physical changes, pulsations, in the star. For extrinsic variables we will see light curves that represent stars in a binary system. In this project we will primarily be determining physical properties of binary systems.

In order to describe extrinsic variables we will assume the simplest case of a binary system. The most photons will reach our telescope when both stars are completely visible. In our case we will start with the cooler star to the right of the larger star. Then as the cooler star travels behind the hotter star, the photons the cooler star is producing will not reach our telescope. The light curve will fall as the cooler star moves behind and the lowest point on the light curve occurs when the cooler star is completely behind the hotter star. Next, the light curve will start to rise again as cooler star moves out from behind the larger star and the light curve will return to the same maximum as when the smaller star started on the left. Now, the cooler star will start to move in front of the larger star. So, the cooler star will block photons emitting from the hotter star and the light curve will again fall. The minimum of this point in the curve will be lower than the previous minimum. Why? Well, in this case we assume the hotter star is brighter than the smaller star. The cooler star emits fewer photons than the hotter star. So, blocking the hotter and brighter star with the cooler and dimmer star produces a minimum lower than case where the telescope can see all of the brightest star and none of the dimmer star. For clarity, being able to see all of the brighter star means more photons will reach our telescope than when we see some of the brightest star and some of the dimmer star. A good example of an eclipsing binary can be seen in figure 7.

Now, for the project I look at several effects which can be seen when observing a binary system. The first is whether or not the system is a contact system. In a contact system the stars are close enough that their atmospheres are combining. The small orbiting radius combined with the sharing of atmospheres creates a light curve with more gradual changes in the light curve as seen in figure 2. Next, from the variation in minimum to maximum magnitude we can determine a luminosity relationship and the inclination:

$$L_{max}/L_{min} = 10^{.4(m_{min}-m_{max})} \text{ goes as } \cos\theta + 1, \tag{6}$$

where $\theta = 90°$ is an edge in view. A similar relation can be determined for the temperatures using

$$L_{max}/L_{min} = (T_1/T_2)^4 = 10^{.4(m_{min1}-m_{min2})}, \tag{7}$$

Additionally I analyze other geometric effects that effect the shape of the light curve. The first is eccentricity (e), or the orientation of the smaller star in relation to the larger star. The smaller star may have an orbit which causes the minima to not be symmetric. This asymmetry can occur if the smaller star has an elliptical orbit relative to our view. This quantity is left out of the tables since none of the binary variables showed any obvious signs of eccentricity. The oblateness of the stars also causes a rounding out of the light curve (Otero et al. 2009). Finally, I used SIMBAD (http://simbad.u-strasbg.fr/simbad/) to determine the parallax (mas) and the color index (B-V). The distance in parsecs (pc) is determined using the SIMBAD data and $d_S = 1/(10^{-3})$. For intrinsic variables I also determined the distance using period luminosity relations given by McNamara et al. (2000).

For δ Scuti I use:

$$M_v = -3.725\ log(p) - 1.933. \tag{8}$$

For R.R. Lyrae I use:

$$M_v = -2.66\ log(p) - 0.33. \tag{9}$$

Finally we calculate the distance (pc) using $d_{pl} = 10^{(m_v - M_v + 5)/5}$.

The light curves deemed variable stars and their physical properties are listed in tables 1, 2, 3. The project yielded a total of 27 variable star curves. Of these 27, 10 were found on all seven nights and able to be phased and can be found in table 1. Two of the stars found on all seven nights and phased were incorrectly classified when compared to SIMBAD. Even though the classifications do not match SIMBAD the curves were left in table 1 as numbers 1, figure 1, and 8, figure 8, since my phasing looks correct. Note, the SIMBAD classification for number 1 reads V* HH UMa – Variable Star of delta Sct type. For table 1 the SIMBAD classification is listed as *().

Table 2 lists two variables that have questionable phasing. Light curve number 1, figure 11 while physically plausible, has large errors which makes the results difficult to trust. Light curve number two, figure 12, was not found on all seven nights and has a period longer than a single night of observation. The resulting plot and data is a good example of incorrect phasing. The phased period

is far different from the visual estimation and the phased curve is not physically realistic. I guessed a classification of δ Cepheid due to the long period.

Table 3 is a list of variable stars that had multiple nights missing and were not phased. Number 15 in table 3, figure 27 was manually identified by me as a δ Scuti. I determined this classification by noticing the shape indicated an intrinsic variable, the short period,$T \approx .07$ days, and the amplitude,$M_{max} - M_{min} = 0.15$. Then I calculated the distance, $d_{pl} = 497$(pc) using the period luminosity relation. Except for the two previously mentioned variable stars, my manual classifications match SIMBAD.

5. CONCLUSION

In conclusion, I was able to learn about δ Scuti pulsations and their frequency analysis. I identified at least one δ Scuti and calculated its distance using period luminosity relations. Additionally, I identified 27 variable stars light curves from ROTSE-I data. Of these 27 variable star light curves I phased 12 and had issues or discrepancies with four. I was able to classify and determined the distance using period luminosity relations for four intrinsic variable stars. Finally, for 27 variable stars I identified relevant physical attributes.

Table 1. Variable Stars found on all 7 nights and phased.

N	RA and Dec	Calc T (days)	Cal Δ M	Est T (days)	Est Δ M	Class.	Eclipse	Incl.	$(T_1/T_2)^4$	Oblate	B-V	Parr. (mas)	d_S (pc)	d_{pl} (pc)
1	J110448.15+353626.5	0.375545	.18	2*0.19	0.18	W U Ma *(DS)	total	83.09°	1.05	···	0.53 [0.04]	3.6745 [0.0446]	272	···
2	J112141.06+433653.0	0.476060	.225	2*0.25	0.26	W U Ma	total	82.7°	1.02	···	0.55 [0.09]	1.6740 [0.0492]	597	···
3	J113536.73+384557.5	0.26971	.406	.27	0.4	R.R. Lyrae	···	···	···	···	0.43 [0.11]	0.5509 [0.0501]	1815	1598
4	J113721.75+425544.7	0.393759	.367	2*0.18	0.35	W U Ma	total	82.1°	1.025	···	0.63 [0.10]	2.7991 [0.0589]	357	···
5	J113334.70+425829.3	0.801011	.279	2*0.3	0.4	Algol	total	···	2.5	yes	0.28 [0.23]	2.2285 [0.0307]	449	···
6	J111305.99+402137.6	0.318005	.314	.25	0.26	R.R. Lyrae	···	···	···	···	0.59 [0.12]	0.5757 [0.0612]	1737	1665
7	J112541.63+423448.9	0.349546	.391	.35	0.41	Algol	partial	···	6.3	some	0.95 [——]	7.4893 [0.0464]	134	···
8	J111615.10+355027.2	0.173405	.368	0.17	0.4	δ Scuti *(W UMa)	···	···	···	···	0.64 [0.28]	2.0978 [0.0686]	1563	···
9	J111716.10+385717.4	0.681234	.256	2*.26	0.24	W UMa	partial	82.8°	1.05	very	···	1.3282 [0.0865]	753	···
10	J113929.00+403633.7	0.523059	.447	.5	0.65	W UMa	partial	80.9°	1.04	yes	···	1.2295 [0.0378]	813	···

Table 2. Variable Stars phased incorrectly.

N	RA and Dec	Cal T (days)	Cal Δ M	Est T (days)	Est Δ M	Classification	Incl.	$(T_1/T_2)^4$	Oblate	B-V	Parr. (Mas)
1	J113011.63+393042.8	0.369188	.102	2*0.21	.15	W UMa	83.9°	1.04	yes	···	
2	J112300.96+380607.9	1.6890204	.124	>.8 days	.1	Poss. δ Cepheid	···	···	···	0.81 [.29]	2.3626 [0.0601]

Table 3. Variable Stars found on Some Nights and Not Phased.

N	RA and Dec	Est T (days)	Est Δ M	Class.	Eclipse	Incl.	$(T_1/T_2)^4$	Oblate	B-V	Parr. (mas)	d_S (pc)	d_{pl} (pc)
1	J110340.85+402617.1	0.15	0.4	W UMa	partial	82.1°	0.91	no	···	1.6555 [0.0367]	604	···
2	J110545.82+361554.0	0.45	0.13	W UMa	partial	80.7°	1.09	no	0.62 [—]	1.6740 [0.0492]	597	···
3	J110550.27+374805.5	0.13	0.2	δ Scuti	···	···	···	···	···	···	···	2272
4	J111345.06+423951.8	0.3	0.2	Algol	partial	···	1.02	yes	0.10 [0.09]	···	···	···
5	J111556.39+373835.2	0.185	0.12	W UMa	some	80.7°	···	···	0.05 [0.03]	5.0651 [0.0521]	197	···
6	J111622.88+411401.0	1.0	0.5	R.R. Lyrae	···	···	···	···	···	0.0819 [0.0411]	12210	7345
7	J111734.14+410649.1	···	0.5	Algol	partial	···	···	no	···	2.4734 [0.0474]	404	···
8	J112148.86+405938.4	.21	0.18	W UMa	partial	83.0°	1.04	···	···	···	···	···
9	J112206.29+375441.9	.3	0.18	W UMa	partial	83.1°	···	···	···	1.6740 [0.0492]	597	···
10	J112944.11+355702.8	.48	0.1	W UMa	partial	83.6°	···	···	1.08 [0.29]	1.3949 [0.0907]	717	···
11	J113028.29+434149.0	.23	0.6	W UMa	partial	80.9°	···	···	···	3.9889 [0.0399]	251	···
12	J113317.93+355438.6	.23	0.3	W UMa	partial	85.8°	···	···	···	0.8372 [0.0298]	1194	···
13	J113458.41+422310.3	$> .4$	0.26	W UM	partial	···	···	···	···	···	···	···
14	J113713.58+362420.0	.32	0.52	W UMa	partial	81.0°	···	···	···	1.5236 [0.0270]	656	···
15	J112037.66+392100.5	.07	0.1	δ Scuti	···	···	···	···	0.10 [0.12]	1.0828 [0.0634]	923	904

REFERENCES

Akerlof, C., Alcock, C., Allsman, R., et al. 1994, ApJ, 436, 787, doi: 10.1086/174954

Balona, L. A., Daszyńska-Daszkiewicz, J., & Pamyatnykh, A. A. 2015, Monthly Notices of the Royal Astronomical Society, 452, 3073, doi: 10.1093/mnras/stv1513

Bertin, E., & Arnouts, S. 1996, A&AS, 117, 393, doi: 10.1051/aas:1996164

Breger, M., Stich, J., Garrido, R., et al. 1993, Nonradial Pulsation of the Delta-Scuti Star Bu-Cancri in the Praesepe Cluster. http://articles.adsabs.harvard.edu/pdf/1993A%26A...271..482B

Collaboration, R., Akerlof, C., Amrose, S., et al. 2000, ROTSE All Sky Surveys for Variable Stars I: Test Fields. https://arxiv.org/abs/astro-ph/0001388

Fagg, E., Park, J., Pearson, K., & Kehoe, R. 2009, General Search for Stars with Rapid Optical Variations: Test Fields, http://www.physics.smu.edu/~kehoe/ugradRes/ms108_111609.pdf

Kehoe, R., Akerlof, C., Balsano, R., et al. 2002, The Astrophysical Journal, 577, 845–852, doi: 10.1086/342231

McNamara, D. H., Madsen, J. B., Barnes, J., & Ericksen, B. F. 2000, Publications of the Astronomical Society of the Pacific, 112, 202, doi: 10.1086/316512

Neilson, H. R., Percy, J., & Smith, H. R. 2016, Period Changes and Evolution in Pulsating Variable Stars, https://arxiv.org/abs/1611.03030

Otero, S., Watson, C., & Wils, P. 2009, Variable Star Type Designations in VSX, https://www.aavso.org/vsots_delsct

Templeton, M. 2010, Delta Scuti and the Delta Scuti variables, https://www.aavso.org/vsots_delsct

6. VARIABLE STAR PLOTS

6.1. *Figures of Phased Variable Stars*

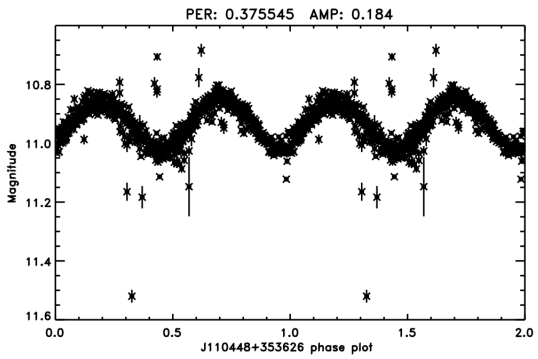

(a)

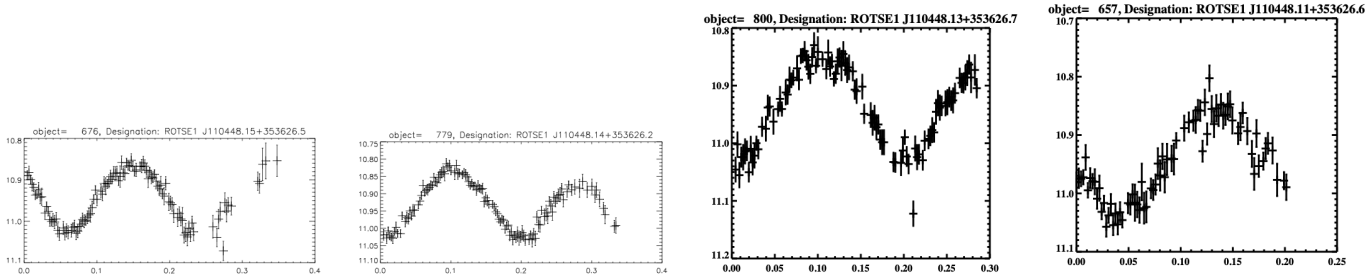

(a) (b) (c) (d)

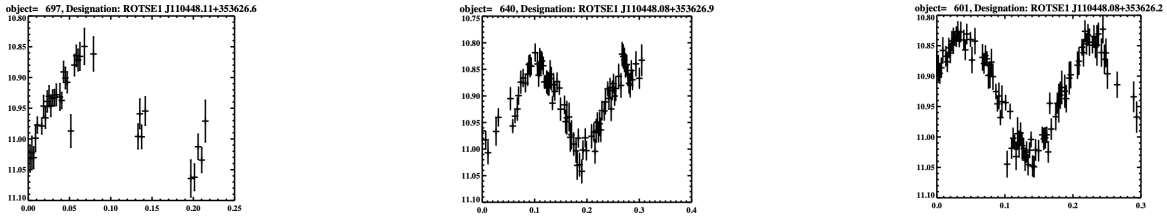

(e) (f) (g)

Figure 1. J110448+353626: Phased (a) and all seven nights (b-d).

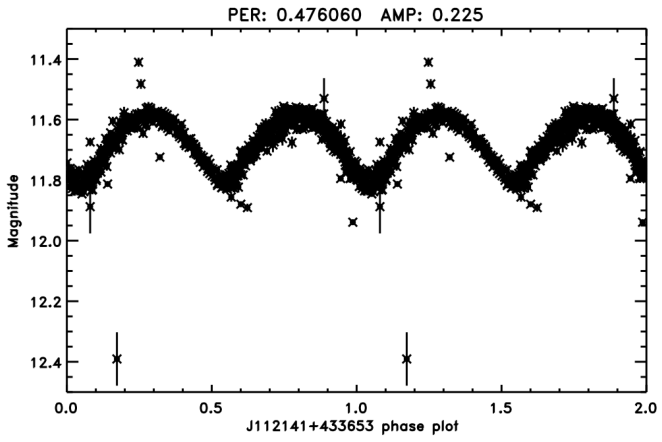

(a)

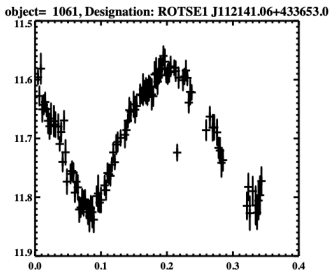

(a)

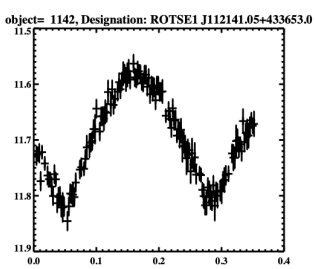

(b)

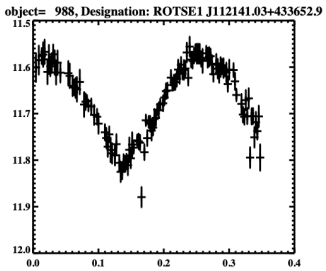

(c)

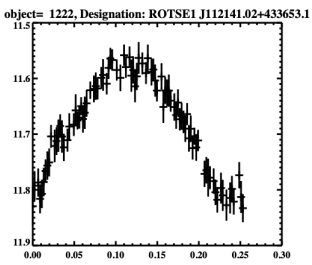

(d)

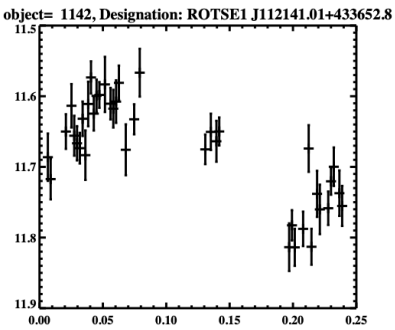

(e)

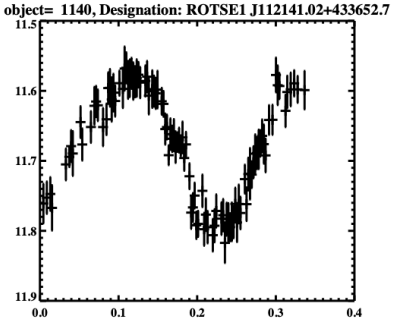

(f)

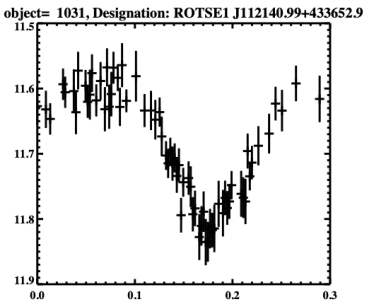

(g)

Figure 2. J112141+433653: Phased (a) and all seven nights (b-d).

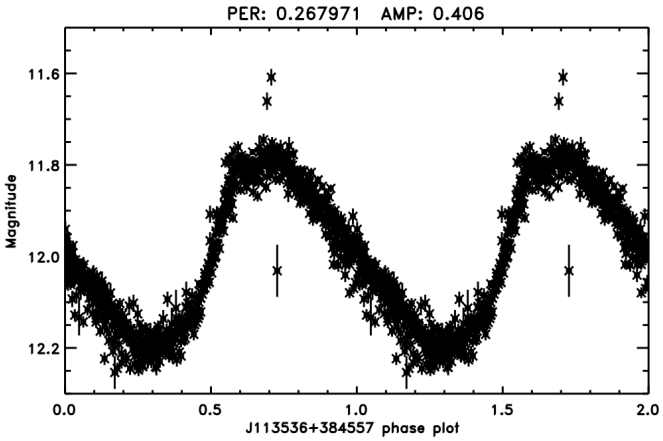

(a)

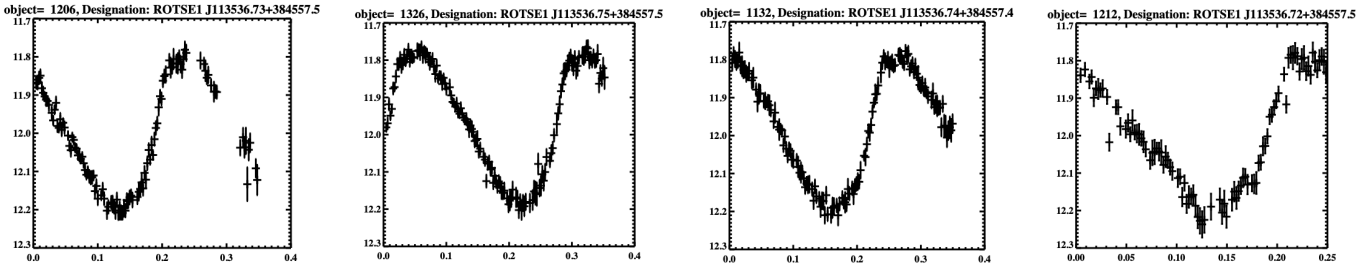

(a) (b) (c) (d)

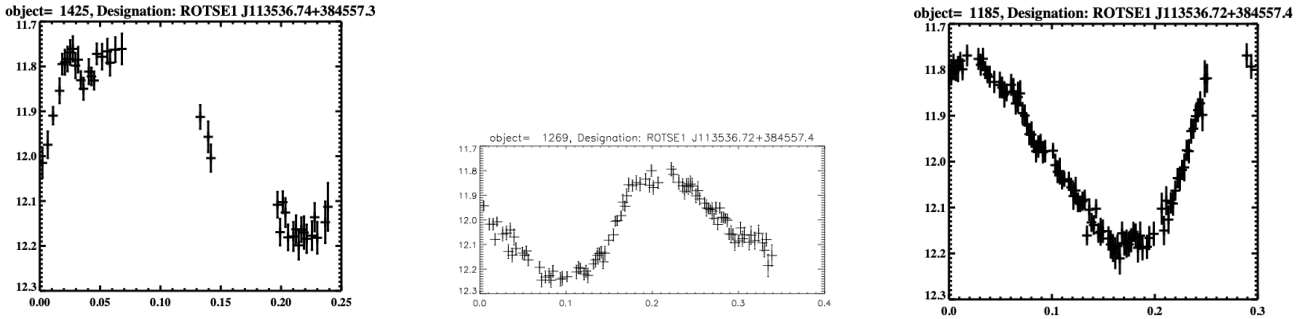

(e) (f) (g)

Figure 3. J113536+384557: Phased (a) and all seven nights (b-d).

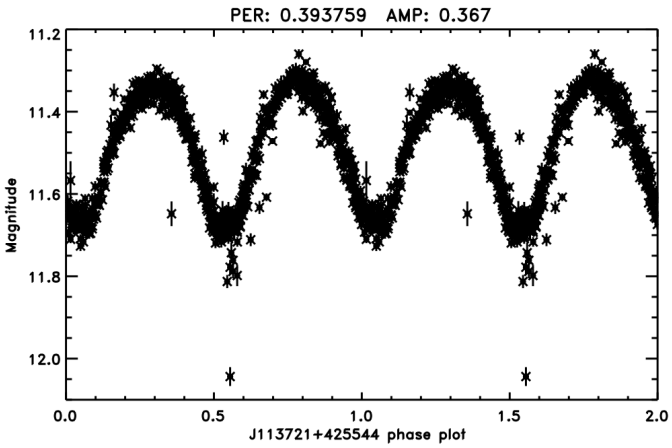

(a)

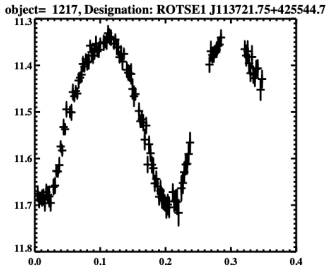

(a)

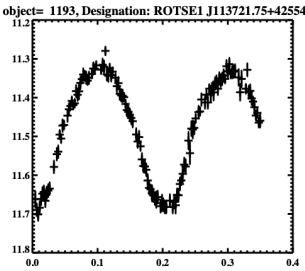

(b)

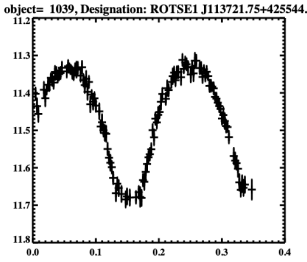

(c)

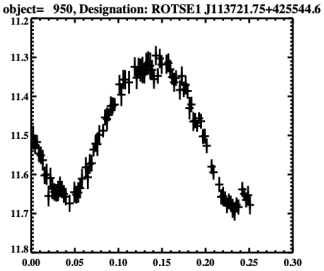

(d)

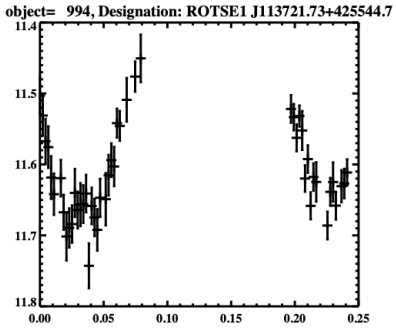

(e)

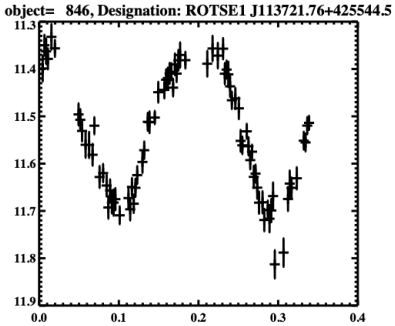

(f)

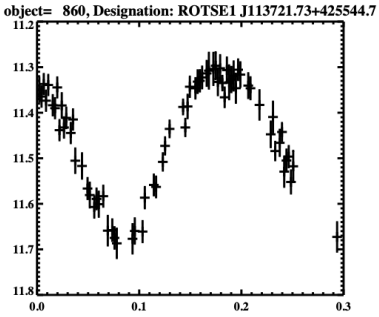

(g)

Figure 4. J113721+425544: Phased (a) and all seven nights (b-d).

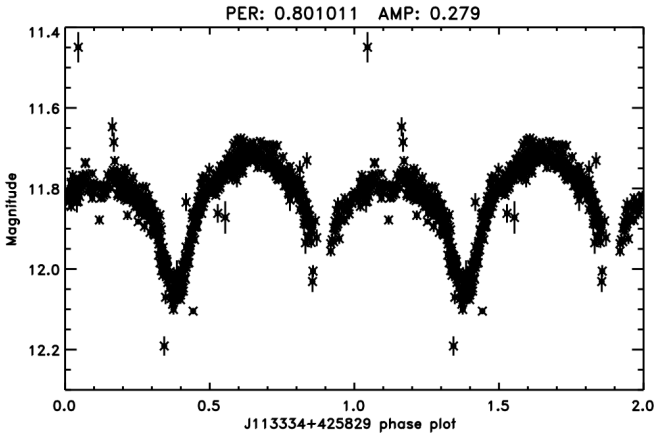

(a)

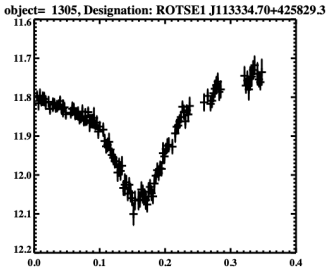

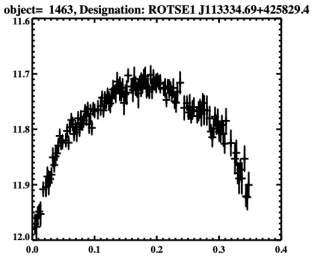

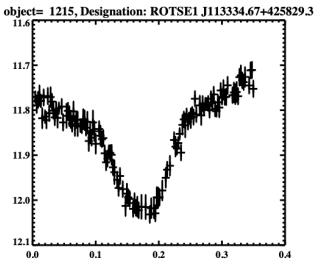

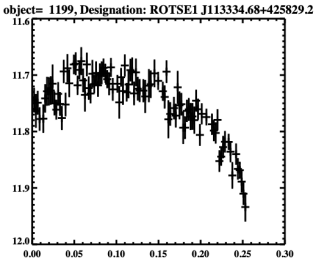

(a) (b) (c) (d)

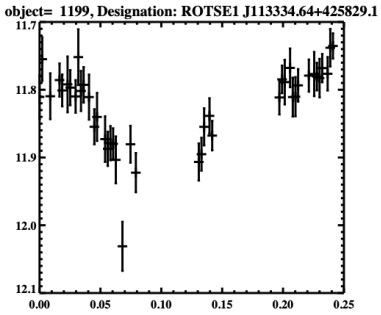

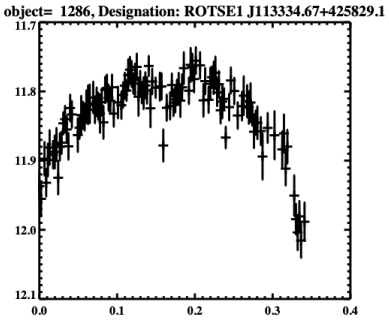

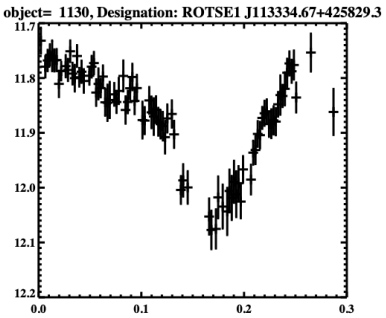

(e) (f) (g)

Figure 5. J113334+425829: Phased (a) and all seven nights (b-d).

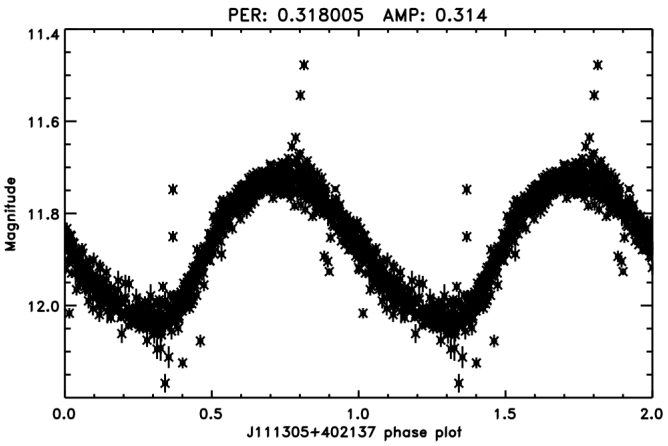

(a)

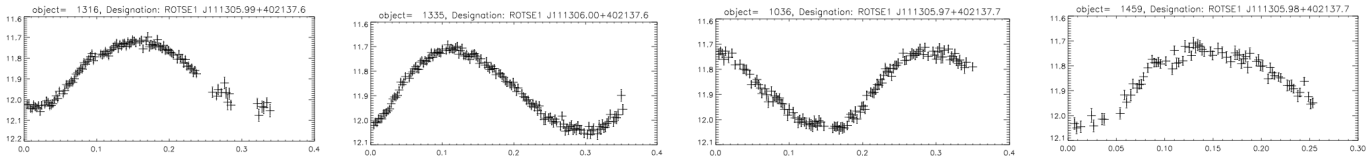

(a) (b) (c) (d)

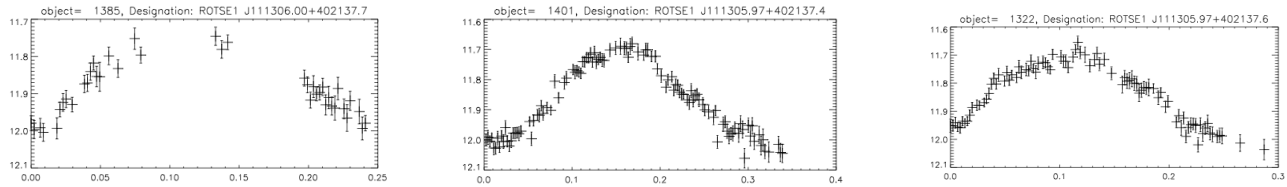

(e) (f) (g)

Figure 6. J111305+402137: Phased (a) and all seven nights (b-d).

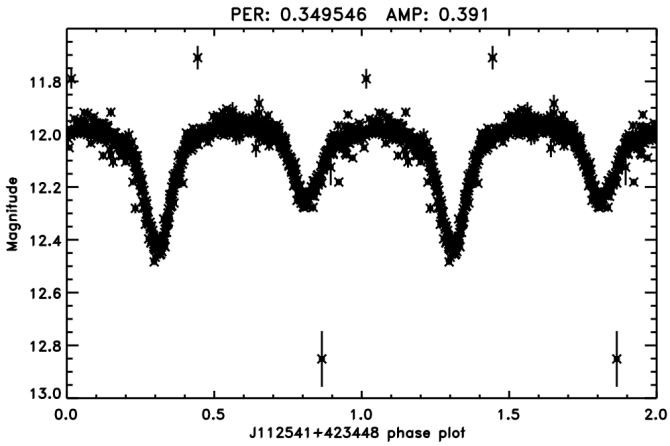

(a)

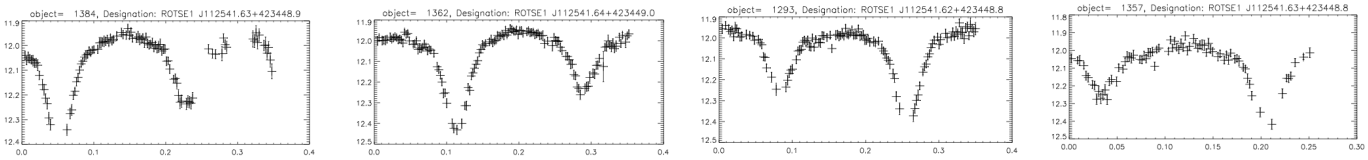

(a) (b) (c) (d)

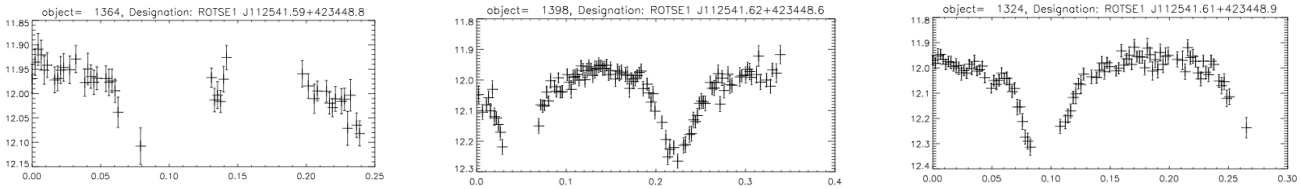

(e) (f) (g)

Figure 7. J112541+423448: Phased (a) and all seven nights (b-d).

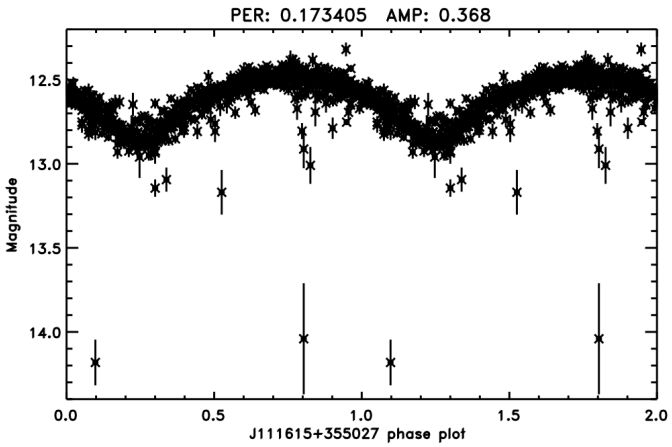

(a)

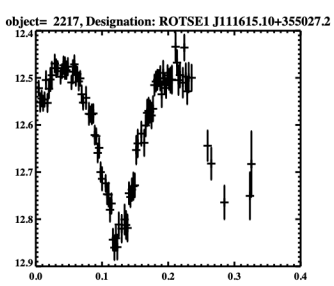

(a)

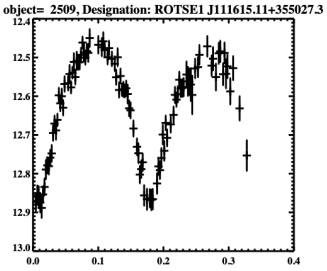

(b)

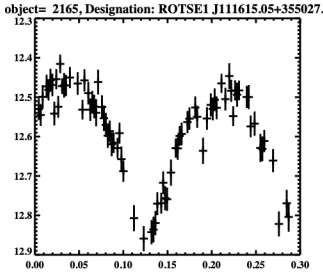

(c)

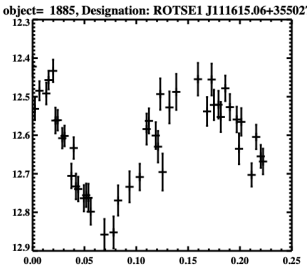

(d)

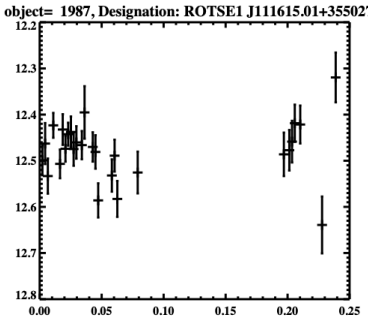

(e)

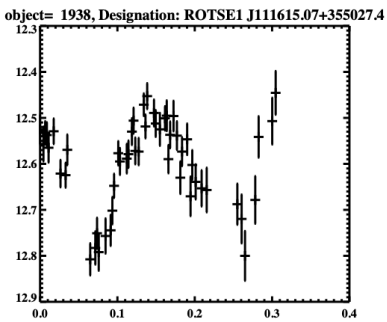

(f)

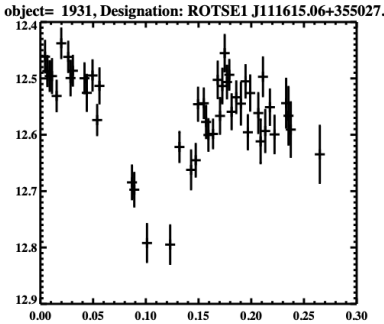

(g)

Figure 8. J111615+355027: Phased (a) and all seven nights (b-d).

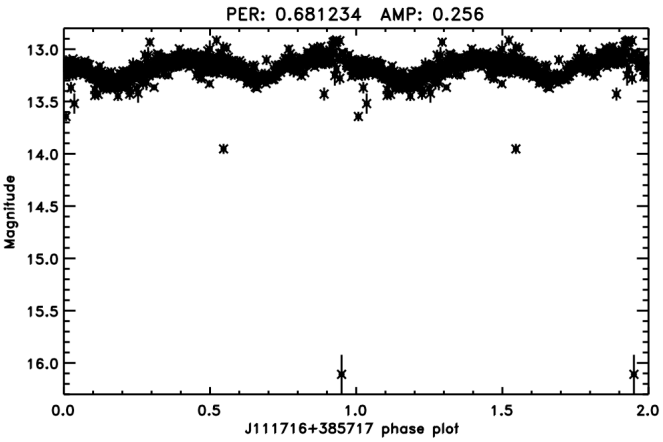

(a)

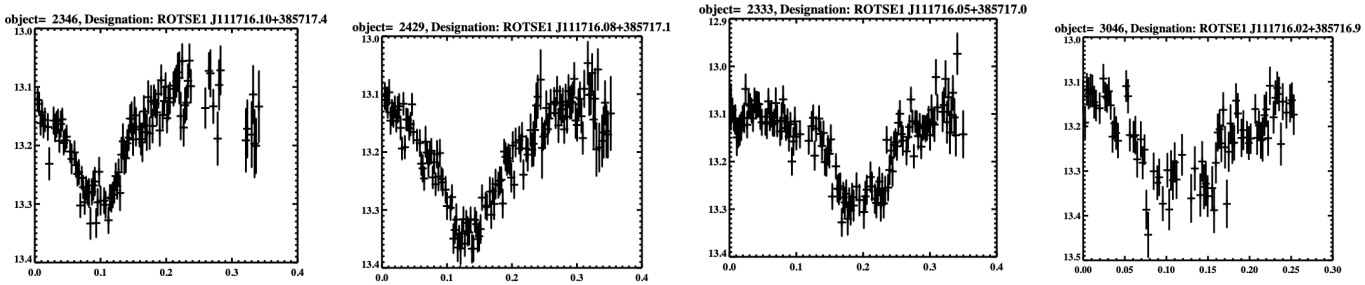

(a) (b) (c) (d)

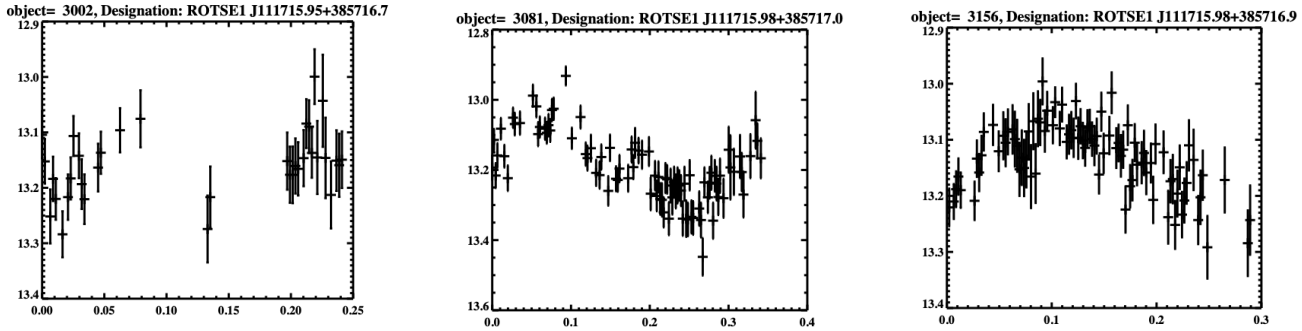

(e) (f) (g)

Figure 9. J111716+385717: Phased (a) and all seven nights (b-d).

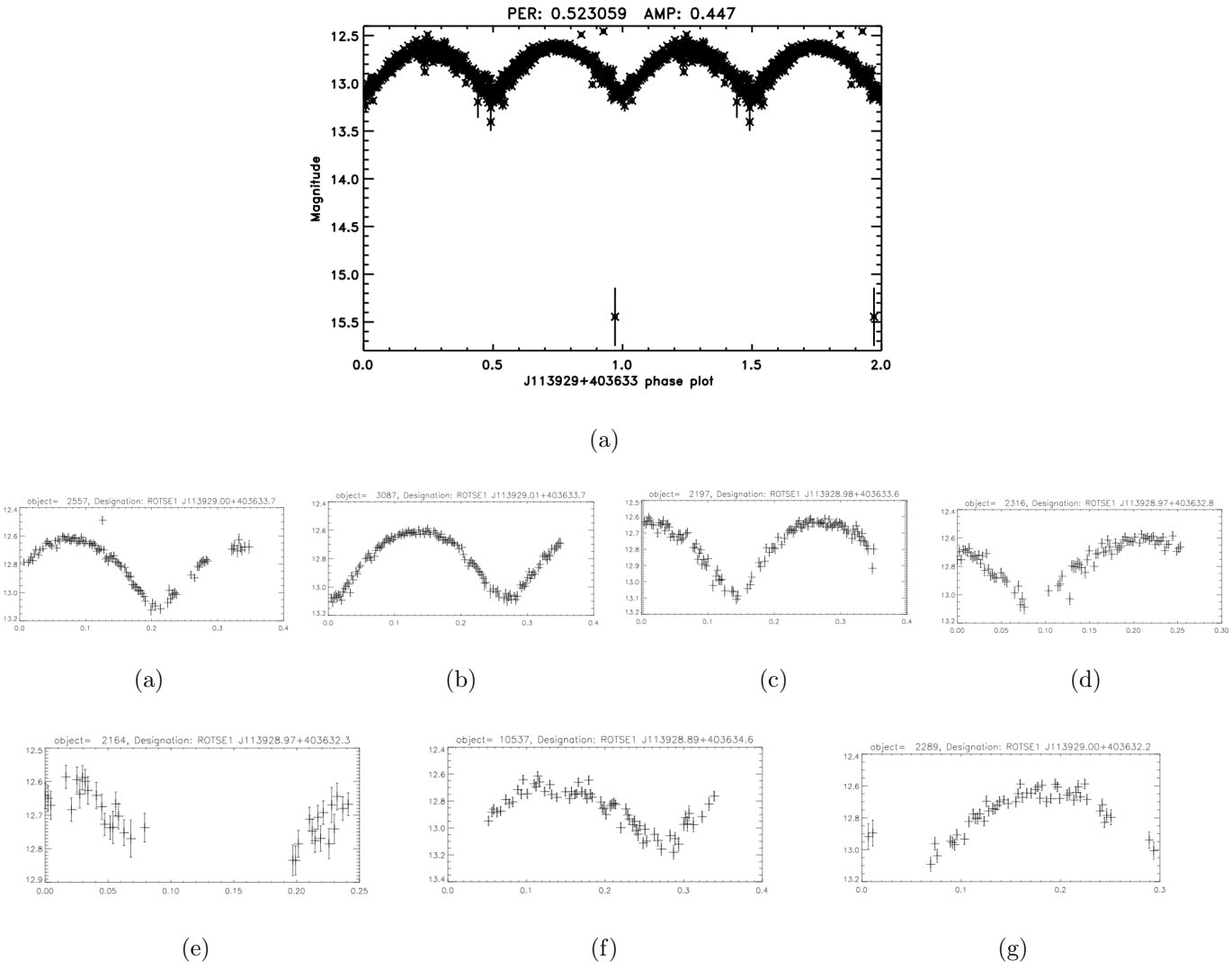

(a)

(a) (b) (c) (d)

(e) (f) (g)

Figure 10. J113929+403633: Phased (a) and all seven nights (b-d).

6.2. *Figures of Incorrectly Phased Variable Stars*

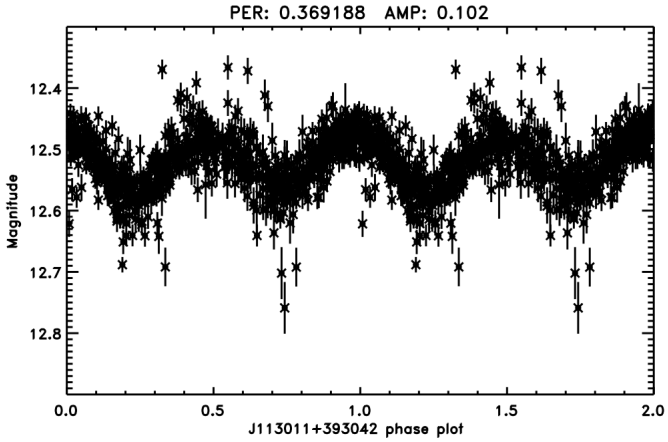

(a)

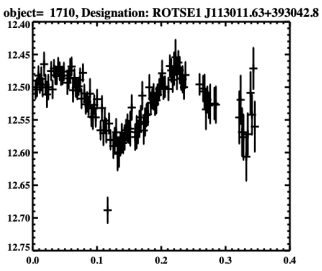

(a)

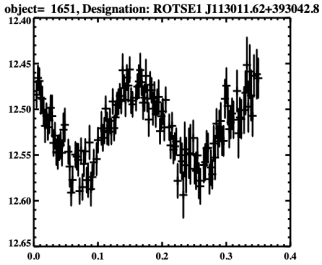

(b)

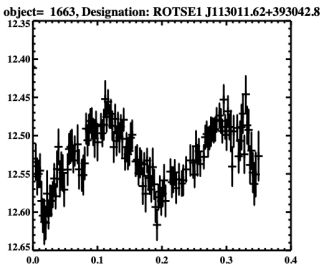

(c)

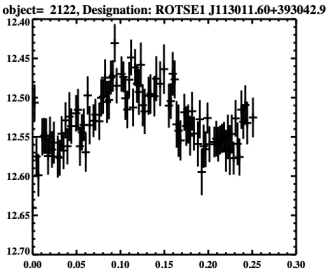

(d)

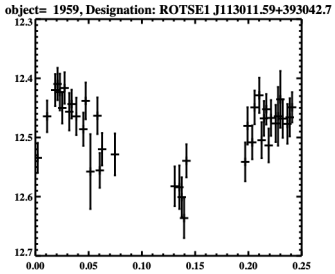

(e)

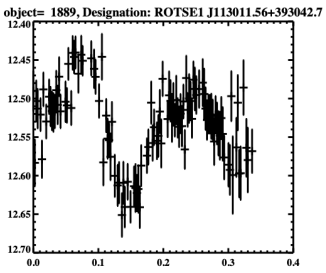

(f)

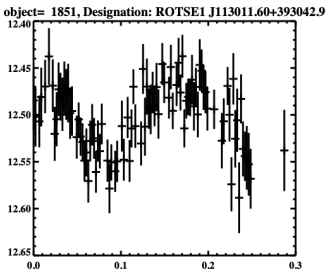

(g)

Figure 11. J113011+393042: Phased and nights 1,2,3,4,5,6,7.

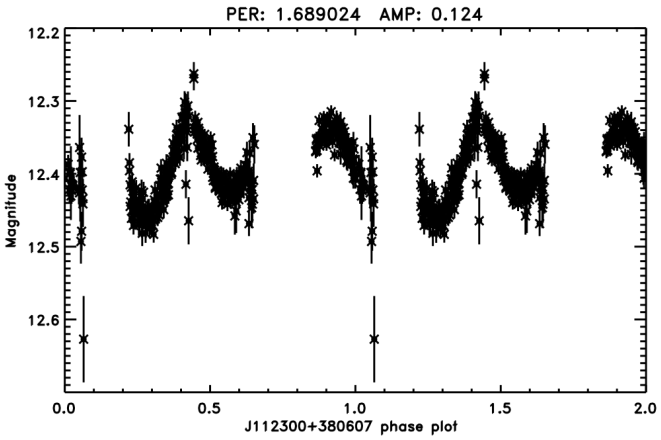

(a)

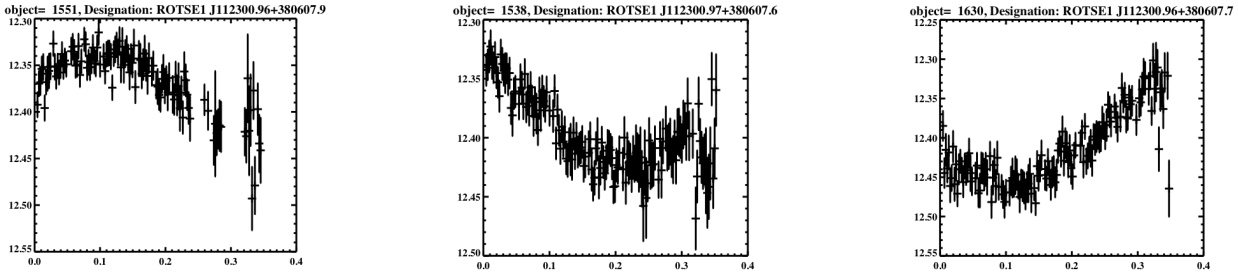

(a) (b) (c)

Figure 12. J112300+380607: Phased and nights 1,2,3.

6.3. *Figures of Variable Stars Not Phased*

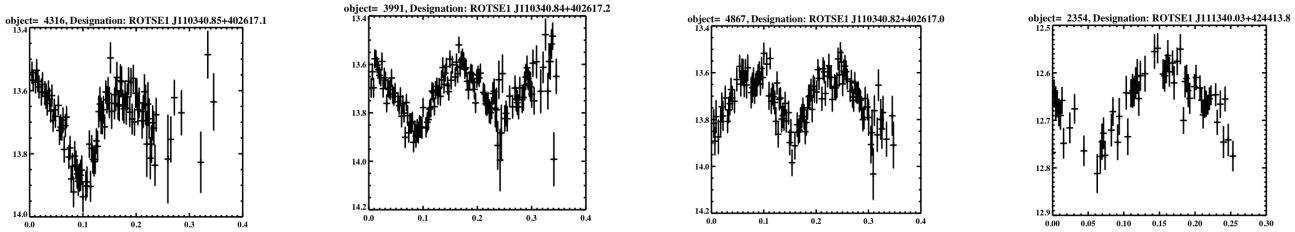

(a) (b) (c) (d)

Figure 13. J110340+402617: Nights 1,2,3,4.

(a) (b)

Figure 14. J110545+361554: Nights 2,3.

(a) (b)

Figure 15. J110550+374805: Nights 6,7.

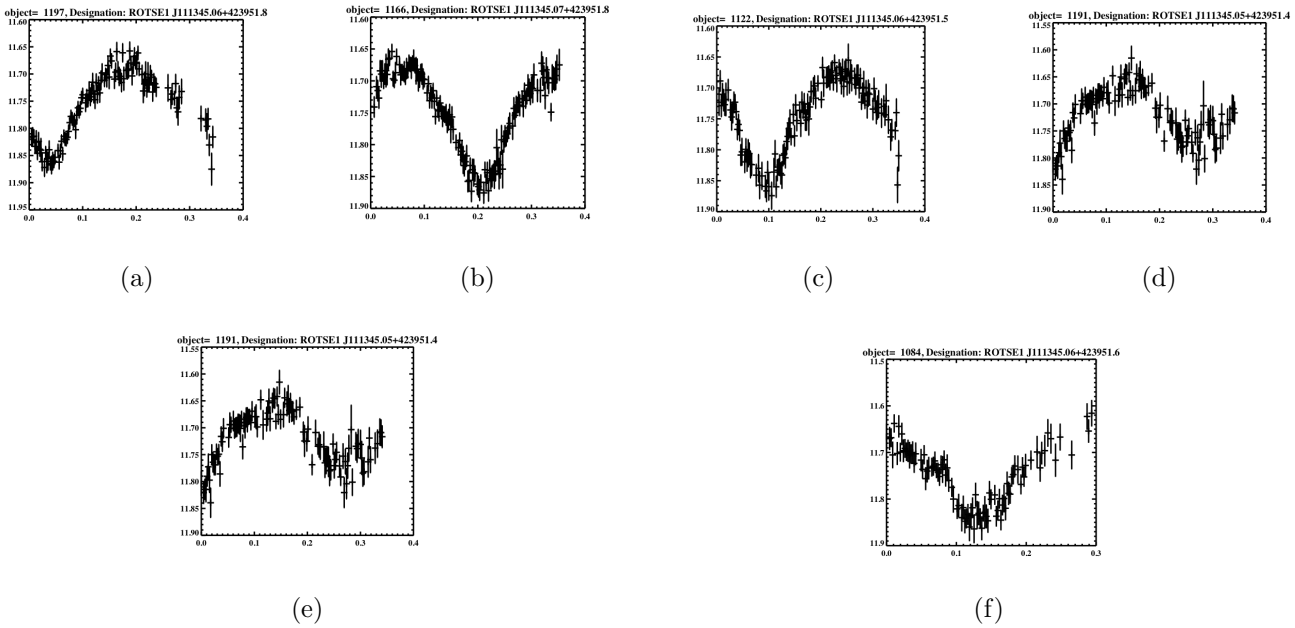

Figure 16. J111345+423951: Nights 1,2,3,4,6,7.

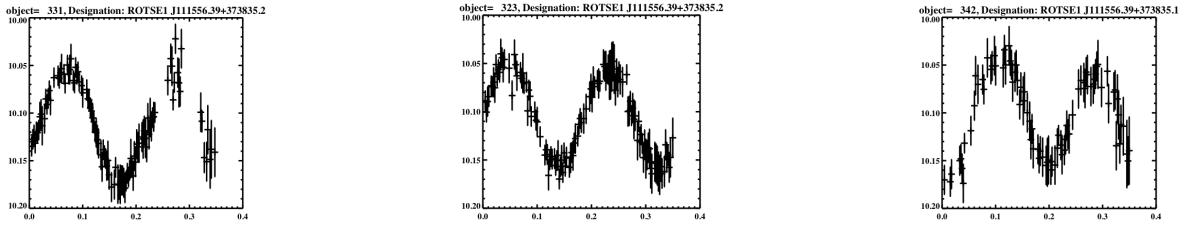

Figure 17. J111556+373835: Nights 1,2,3.

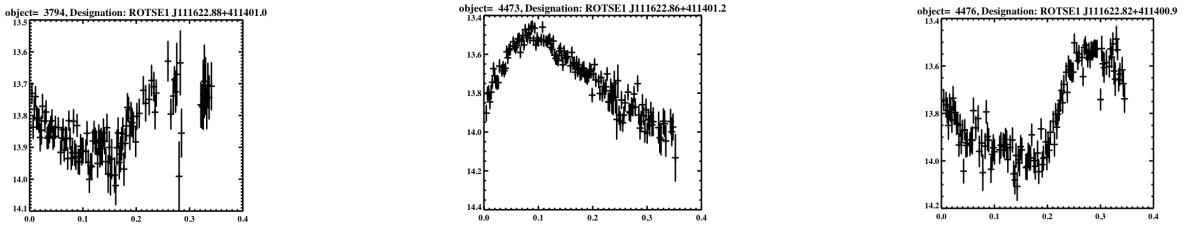

Figure 18. J111622+411401: Nights 1,2,3.

(a) (b)

Figure 19. J111734+410649: Nights 1,4.

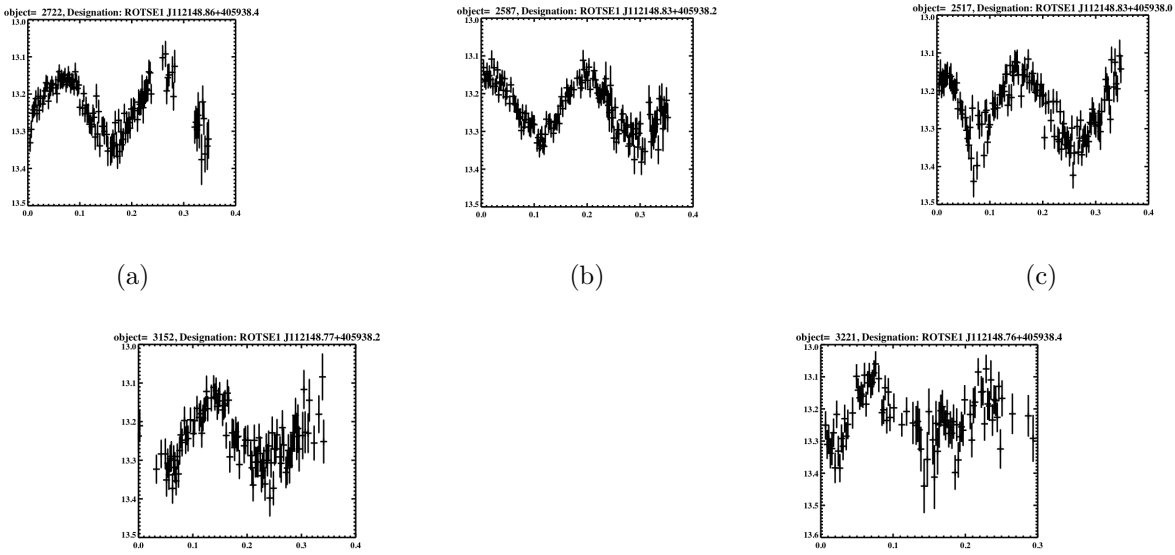

(a) (b) (c)

(d) (e)

Figure 20. J112148+405938: Nights 1,2,3,4,7.

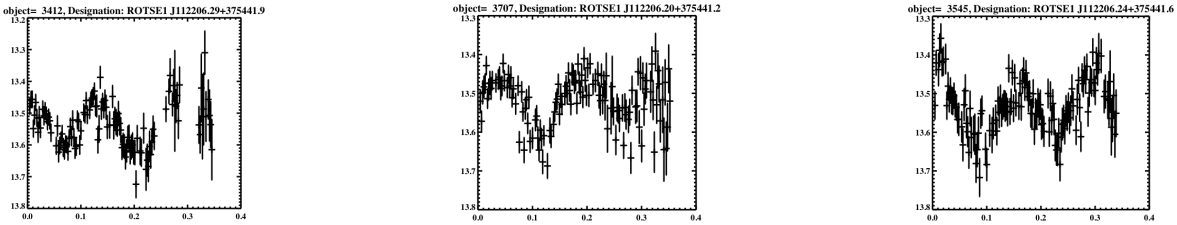

(a) (b) (c)

Figure 21. J112206+375441: Nights 1,2,3.

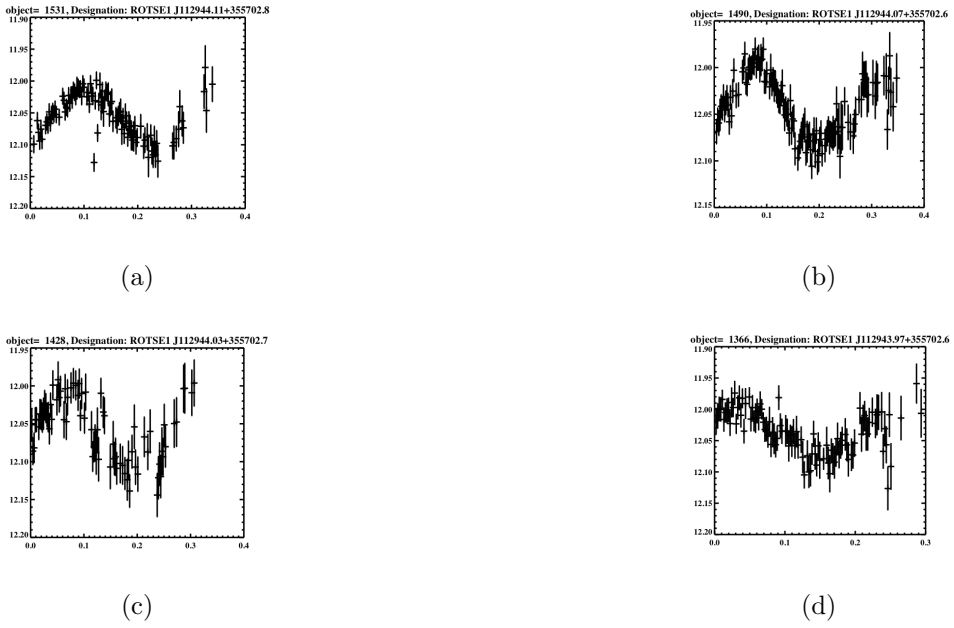

(a) (b)

(c) (d)

Figure 22. J112944+355702: Nights 1,2,6,7.

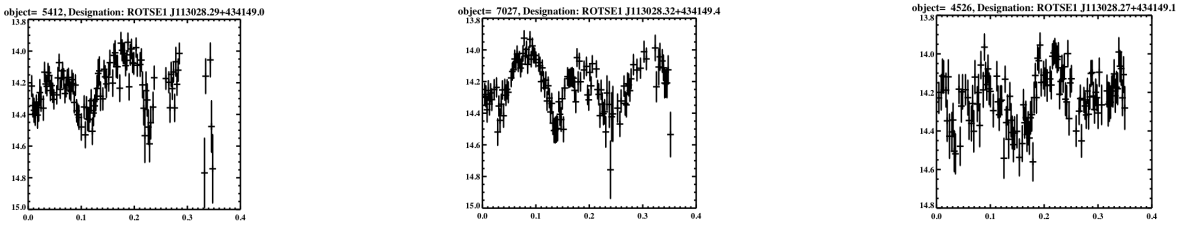

(a) (b) (c)

Figure 23. J113028+434149: Nights 1,2,3.

(a) (b)

Figure 24. J113317+355438: Nights 1,2.

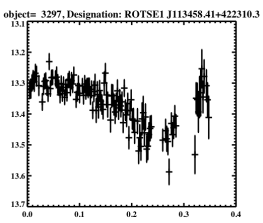

(a)

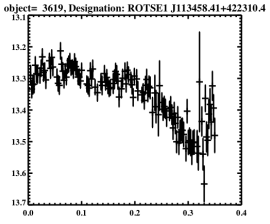

(b)

Figure 25. J113458+422310: Nights 1,2.

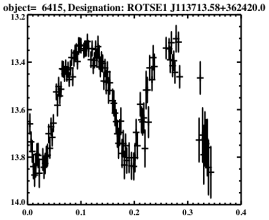

(a)

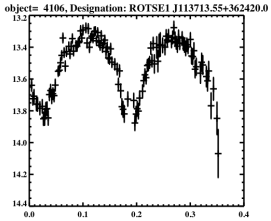

(b)

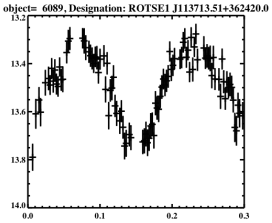

(c)

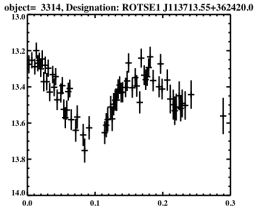

(d)

Figure 26. J113713+362420: Nights 1,2,3,7.

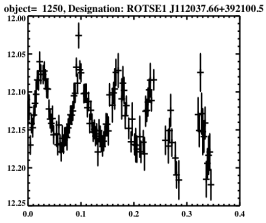

(a)

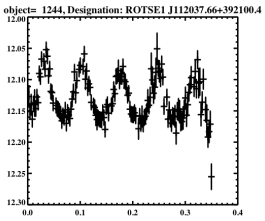

(b)

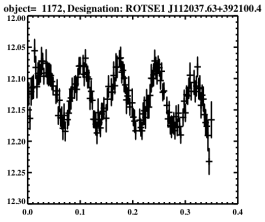

(c)

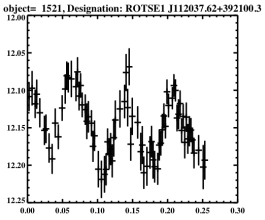

(d)

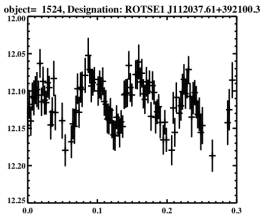

(e)

Figure 27. J112037+392100: Nights 1,2,3,7.